

International Conference on Space Optics—ICSO 2018

Chania, Greece

9–12 October 2018

Edited by Zoran Sodnik, Nikos Karafolas, and Bruno Cugny



High-performance DFB laser module for space applications: the FP7 HiPPO achievements from chip fabrication to system validation

M. Faugeron

B. Benazet

A. Maho

A. Le Kernec

et al.



High-performance DFB laser module for space applications: the FP7 HiPPO achievements from chip fabrication to system validation

M. Faugeron^{*a}, B. Benazet^a, A. Maho^a, A. Le Kernec^a, M. Sotom^a, F. van Dijk^b, J-P. Le Goëc^b, O. Parillaud^b, L. Stampoulidis^c, P. Henderson^c, S. Snowden^c, E. Kehayas^c
^aThales Alenia Space, 26 av. J.-F. Champollion, 31037 Toulouse, France; ^bIII-V Lab, 1 av. A. Fresnel, 91767 Palaiseau, France, ^cGooch&Housego, Broomhill Way, Torquay TQ2 7QL, UK

*mickael.faugeron@thalesaleniaspace.com; phone 00 33 5 34 35 79 36; www.thalesgroup.com/en/space

ABSTRACT

This article reports the development of 200-mW 1.55- μm DFB laser module with RIN below -162 dB/Hz which are well suited for microwave photonics or free space optical communication applications. Specific design has allowed reaching high power (> 300 mW), low noise and high spectral purity laser chip. The chip has been packaged in Butterfly module optimized for reducing the module power consumption. DFB laser module system validations have been done on three laboratory test-beds representative of target applications, namely high-frequency optical LO distribution, photonic RF frequency conversion, and free space optical communication links.

Keywords: High power DFB laser, photonic RF processing, laser communications

1. INTRODUCTION

In the last decade, Thales Alenia Space and partners have put lots of research efforts in photonic technologies for satellite applications¹. The objective is to provide innovative solutions for improving space-based telecommunication payloads and systems in terms of functionality, capacity, performance and cost. The paper presents the achievements in the development of low-noise, high-power CW distributed feedback (DFB) laser modules in the frame of the FP7-HiPPO (High-Power Photonics for satellite laser communications and On-board optical processing) project. Such laser sources are essential devices for future photonic RF payloads and optical communications systems. In the following sections, we report on the different steps from the laser chip design and fabrication, to the system validation of the performance of packaged modules.

2. DFB LASER CHIP DESIGN, FABRICATION AND PERFORMANCE

The multiple quantum well DFB structure was grown by Gas-Source Molecular Beam Epitaxy (GS-MBE) on *n*-InP substrates. The structure has an asymmetrical cladding and the active region is composed of 6 undoped InGaAsP quantum wells with a 1.54 μm photoluminescence peak. More details about the laser chip design can be found in ^{2[2]}. First order gratings were defined by e-beam lithography and inductively coupled plasma reactive ion etching. The grating layer thickness is optimized in order to obtain a coupling strength $KL \sim 1.2$ for a 1.5 mm cavity length. This low value of KL should limit spatial hole burning and the associated optical power saturation. Re-growth of p-doped top cladding was then also done by GS-MBE. The dual-channel laser ridge-waveguide were formed by ion beam etching followed by wet chemical etch and proton isolation. The ridge-waveguide are 3.5 μm wide. This value was found to minimize the thermal saturation while preserving lateral single-mode operation. Bars were cleaved to form 1.5 mm-long cavities. Facets were High Reflectivity and Anti Reflectivity coated. Chips cleaved from the bars were mounted p-side up on Aluminum Nitride sub-mounts.

Chip measurements were performed at 25°C. The continuous output power of the laser as a function of the current is shown in Figure 1 (left). An output power higher than 100 mW was obtained at 400 mA. The maximum output power was 319 mW at 1.236 A. For a current ramp of 0-800mA at 25°C, the output power shows a good linearity with a limited influence of thermal rollover. Figure 1 (left) inset shows the optical spectra at 200 and 1000 mA with a peak respectively at 1562.9 nm and 1565.2 nm. The side-mode-suppression-ratio (SMSR) is better than 55 dB for both bias currents. Relative intensity noise (RIN) measurements were performed at different bias currents. Plots are given in Figure 1

(right). At 600 mA, the RIN is below -160 dB/Hz in the 0.1-20 GHz range with a relaxation frequency of 6 GHz. At 1000 mA, the RIN is below -165 dB/Hz in the 0.1-3.5 GHz range and below -162 dB/Hz in the 0.1-20 GHz range.

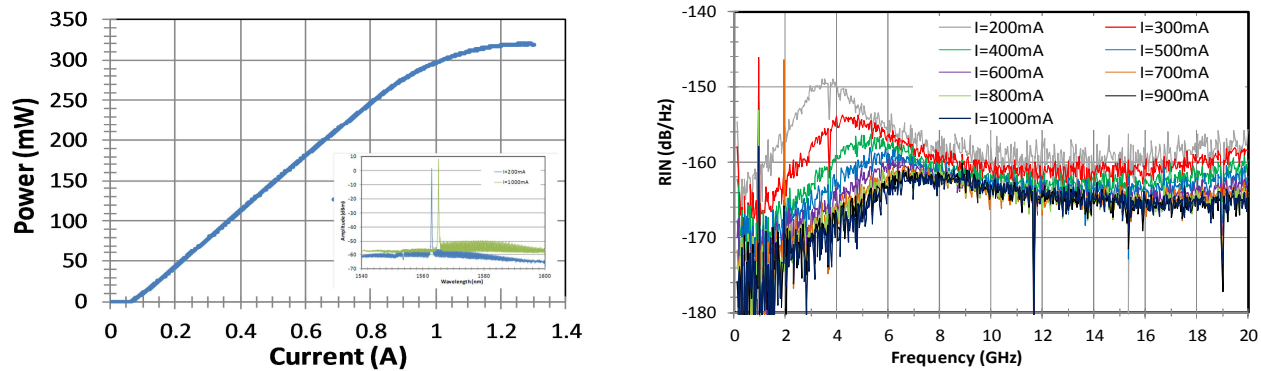


Figure 1. DFB laser chip: (left) Power vs. bias current for a 1.5 mm-long DFB laser and optical spectra at 25°C at 200 and 1000 mA, (right) laser RIN at different bias currents.

For many applications, a narrow laser linewidth is very important. For coherent detection system at 10 Gbps, a reasonable limit is 1 MHz³. A delayed self-heterodyne method was used with 6 km SMF length and a 80 MHz acousto-optical modulator to characterize our device and a low noise current source for the laser bias current. According to⁴, this length is sufficient to work in the incoherent regime for optical linewidth larger than 45 kHz.

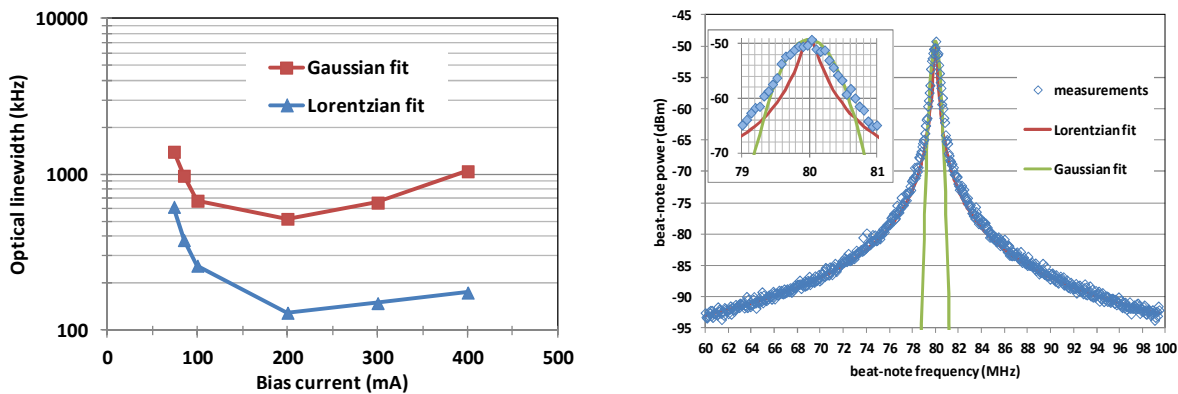


Figure 2. Laser linewidth: (left) Linewidth vs. bias current, (right) Measured beat-note at 200 mA bias current, inset shows a zoom close to the peak.

The Gaussian lineshape is fitted at -3 dB and represents the frequency jitter of 1/f noise of the source⁵ which depends on the interferometer delay (fiber length). The Lorentzian profile represents the white noise and is fitted at -30 dB. Figure 2 (left) presents the linewidth measurements according the two type of fits for a bias current up to 400 mA. The beat-note spectrum used to extract the data is presented in Figure 2 (right). The reduction of the linewidth from the laser threshold current up to 200 mW is due to the increase of the optical power inside the laser cavity. The re-broadening of the linewidth above 200 mA is attributed to the non-uniform optical power density inside the optical cavity that causes spatial hole burning. At 25°C and for a bias current of 200 mA, our 1.5 mm long device exhibits its minimum optical linewidth value of 130 kHz and 520 kHz FWHM respectively for Lorentzian and Gaussian profile.

3. LASER MODULE DEVELOPMENT & TESTING

3.1 Laser module assembly and test plan

Figure 3 (left) shows a fully hermetic packaged and pigtailed 14-pin butterfly DFB laser module prototype. Eight of these modules were assembled and packaged by G&H using hi-reliability module assembly processes. The eight DFB

chips originate from different epi designs and as such DFBs exhibited performance variations including different optical power, linewidth and beam divergence. The DFB parts were delivered as Chip-on-Carrier (CoC) devices and G&H performed the optical bench assembly that contained the DFB CoC aligned to collimating optics, free space isolator and fiber pigtail. The fiber pigtail was mounted using laser welding and the module was packaged using epoxy-free seam sealing for enhanced reliability. The assembly also included a thermo-electric cooler (TEC) for temperature control and an internal photodiode for monitoring the DFB chip output power. Figure 3 (right) shows the in-fiber optical power as a function of driving current (L-I curve) for the eight DFB modules. The modules exhibit an output power ranging from 60 mW up to 97 mW at a maximum driving current of 500 mA and at 25°C. A power consumption as low as 3 W at 500 mA driving current and 25°C was achieved. The module-to-module threshold current and output power variation is partially due to the different DFB laser designs - as explained above. In the past we have shown minimal module-to-module variations when DFB chips from the same design and same lot are used ⁶.

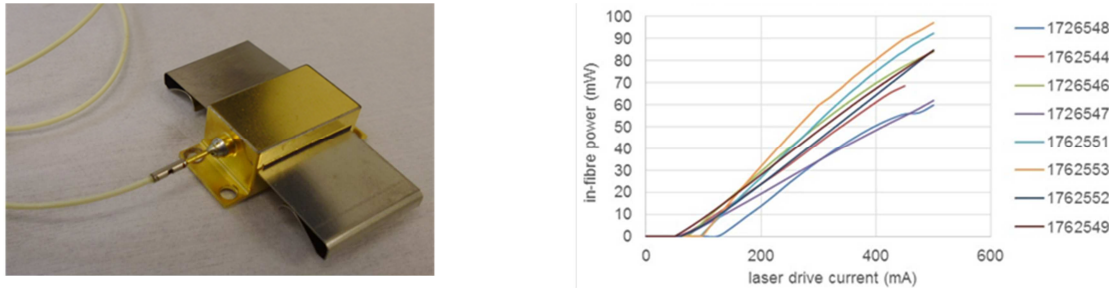


Figure 3. DFB laser module: (left) prototype view, (right) output power vs. drive current for eight modules

During production the modules are subjected to a number of in-process tests that comply with ESCC 23201 qualification test programs for laser diodes. The in-process tests include gross/fine leak, high temperature bake-in, temperature cycling, burn-in and external visual inspection. Following initial functional test prototype devices were tested against proton radiation and high level sine vibration.

3.2 Proton radiation test

One DFB laser module was tested against non-ionizing radiation. With respect to laser diodes the degradation due to displacement damage is expressed through a threshold current shift. The tests have been performed in collaboration with ALTER using the proton radiation facility at UCL. Figure 4 illustrates the test conditions and the device under test. The device has been used through the three different steps until a cumulative dose of 10^{12} p/cm². The device was unbiased during beam exposure. The figure below shows the test conditions and the device under test.

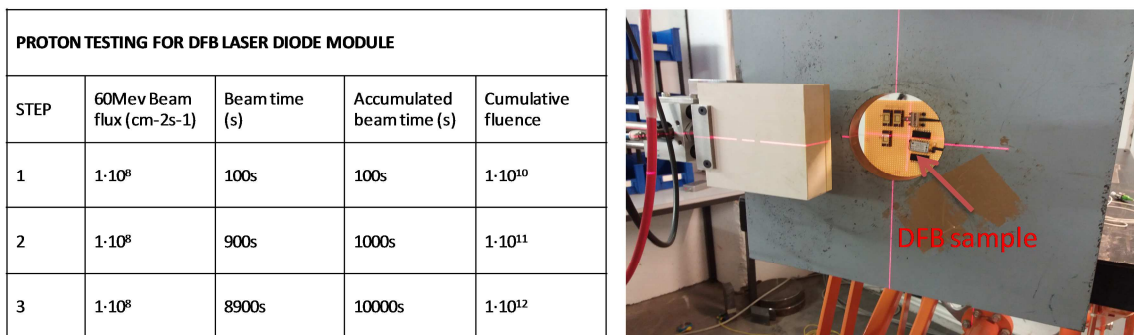


Figure 4. (left) proton radiation test conditions, (right) DFB sample under proton beam irradiation

At each step the device was characterized against: a) the center wavelength at 350 mA driving current, b) the L-I curve at 0-350 mA driving current range and at a current step of 5 mA and c) the internal back-facet monitor dark current and photo-current at a reverse bias of -5V and at 0-350 mA driving current range.

Figure 5 (left) illustrates the L-I curve at initial and intermediate measurement steps. L-I measurements show that there is no detrimental impact on the laser threshold current and efficiency performance with a very good matching of the initial

and intermediate curves. The inset illustrates the measurements of the optical spectrum that show a stable centre wavelength performance.

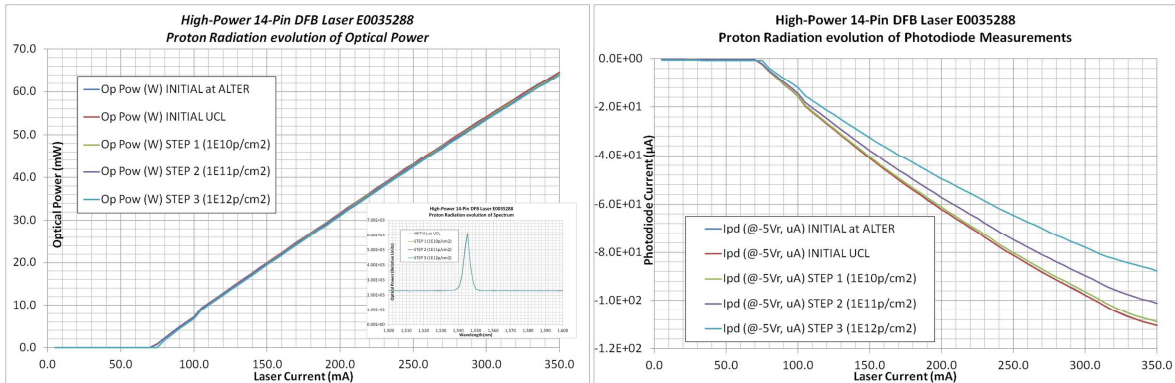


Figure 5. (left) L-I curves at initial, step 1, 2 and 3 of proton radiation. The inset shows the OSA trace at the various measurements points (right) dark current and photo-current evolution as a function of laser diode driving current.

Figure 5 (right) illustrates the back facet monitor dark and photo-current as a function of the DFB laser driving current in the four measurement test steps. The back facet monitor dark current (point of 0 mA laser current on the curve) shows no indication of increase throughout the test. The photo-current is quite stable at step-1 and decreases at step 2 and step 3. The photo-current decrease becomes more pronounced with the increase of the laser driving current with the maximum decrease (obtained at 350 mA) being 8% at step 2 and 20.36% at step 3.

3.3 High level sine vibration test

One sample was subjected to a high level sine vibration test to evaluate the integrity of the optical coupling mechanism. The test condition complied to Telcordia GR-468-CORE test specification which is based on MIL-STD-883D Method 2007.2, Test Cond. A, 20g, 20 Hz to 2000 Hz, 4 minutes per cycle, with 4 cycles for each axis. Figure 6 (left) shows test set-up for high level sine vibration on the out-of-plane axis. The use of the mounting cube allowed to test on the in-plane axis without modification of the shaker arrangement as shown in the figure below (middle). Figure 7 (right) shows the L-I curve result obtained during the critical (out-of-plane axis) testing. The comparison between initial and post-test measurements show a maximum increase of the module optical output power of 19% measured at 450 mA, which is satisfactory for a prototype quality level device. The device was also tested against its wavelength stability and noise performance. The results are given in Table 1.

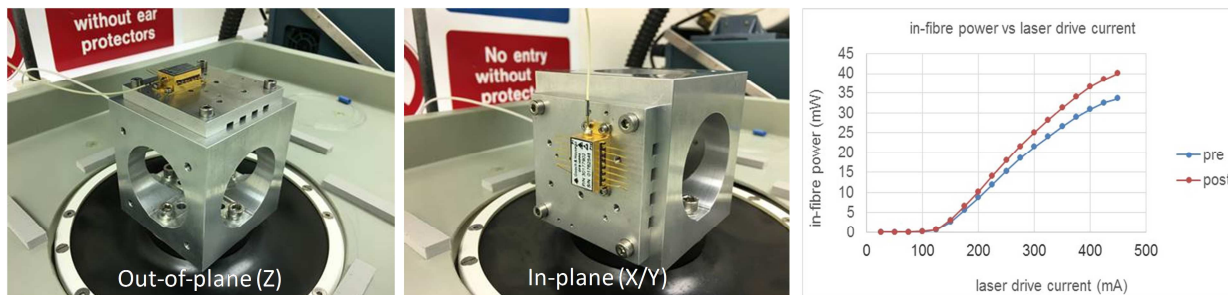


Figure 6. (left & middle) DFB laser module on vibration shaker, (right) L-I curves pre and post vibration

Table 1. DFB laser module output power, wavelength stability and noise performance under high-level sine vibration

Item	Pre-test data	Post-test data
Optical output power at 450mA	33.7 mW	40.1 mW
Wavelength at 450mA	1552.76 nm	1552.75 nm
Wavelength shift with chip temperature	119 pm/C	119 pm/C
RIN	-150 dB/Hz	-150 dB/Hz

4. LASER MODULE PERFORMANCES

The output power as a function of the bias current is plotted in Figure 7 (left). The module threshold current is consistent with the one measured on the chip. The coupling ratio is about 60 %. The laser module exhibits 200 mW for 1130 mA bias current and saturates at 1200 mA. The module exhibits single-mode operation with SMSR higher than 50 dB whatever the bias current as shown in Figure 7 (left) inset.

The module exhibits very low RIN as shown in Figure 7 (right). From 500 mA bias current, the RIN is below -160 dB/Hz on the entire [0.1-20 GHz] range. For larger bias currents, it goes down below -170 dB/Hz up to 3 GHz. In the same way, the agreement between chip and module RIN performances is very good.

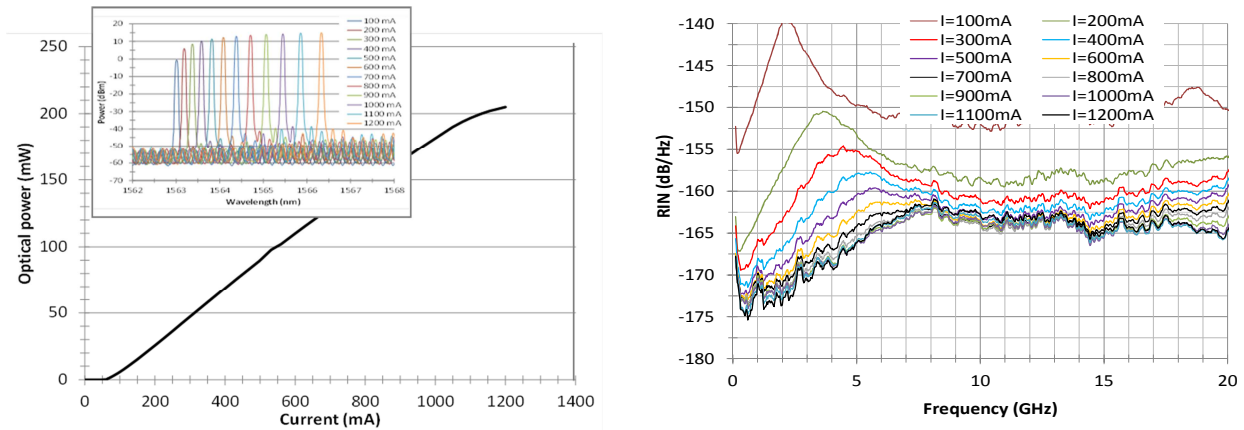


Figure 7. DFB laser module characteristics: (left) Power and optical spectrum vs. current, (right) RIN curves.

5. SYSTEM VALIDATION

The DFB laser performance was assessed in system test beds representative of photonic RF processing and laser communications applications. More specifically, this includes high-frequency LO (local oscillator) distribution, photonic RF frequency conversion and high data rate, free space optical communication links.

5.1 High-frequency LO distribution

The distribution of a centralized LO is a key function in telecom payloads as a single LO can be to many the elements with the same phase, which is important in case of active antennas for instance. When a very stable LO is required for RF frequency conversion, only one ultra-stable source is needed which reduces the cost compared to having one ultra-stable source per mixer. Also, it enables to reduce the mass and complexity of mixers. This distribution can be performed either by RF or by optical solutions. Optical solutions offer the advantages of harness simplification and mass reduction as well as electromagnetic immunity, at the expense of extra power consumption. A key requirement is not to degrade the RF signal purity expressed in terms of phase noise level. For ultra-high-purity signals, any small degradation due to the optical link can be observed, but for high-frequency LO (> 10 GHz), optical distribution becomes very promising because the spectral purity of the RF signal is not degraded and also because the RF losses of coaxial cables at high frequencies make RF solutions unpractical. Figure 8 shows the optical LO distribution set-up developed for a previous project. It includes a high-power laser, a Mach-Zehnder electro-optical modulator (MZM), a variable optical attenuator to create optical loss in relation with the distribution rank and a photodiode. The purpose of this demonstration is to assess the benefits of having a very high output power DFB laser. A commercial +20 dBm, low-noise DFB laser (G&H AA1406) was replaced by one HiPPO laser module delivering +22 dBm output power (power limitation at the MZM input). The MZM was biased at the quadrature ($V_{\pi}/2$) and fed by a RF synthesizer delivering a low-noise RF signal at 30 GHz with an RF power of +20 dBm, which is representative of an LO application in Ka-band satellite payloads.

The output RF power was first measured as a function of the distribution rank. The very-high-power HiPPO laser was shown to increase by a few dB's the RF power available at the photodiode output. The RF phase noise was then measured for distribution rank from 4 to 128, i.e. optical losses from 7 to 24.5 dB.

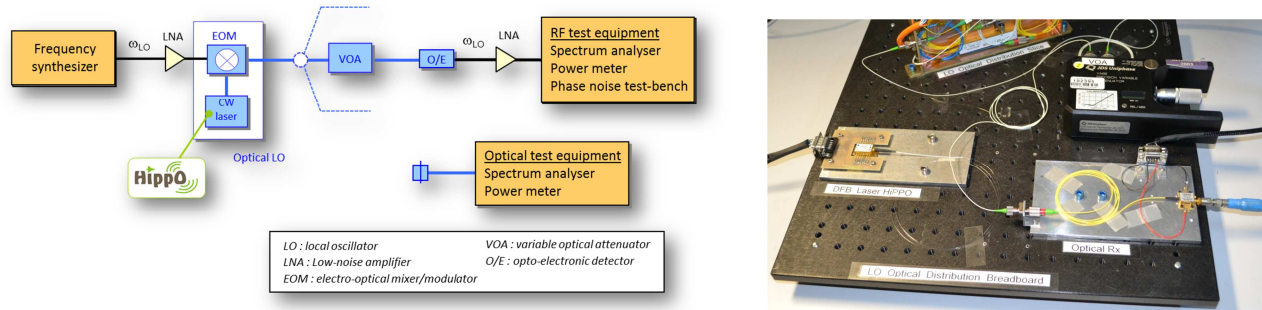


Figure 8. Optical LO distribution set-up: (left) block diagram, (right) picture.

Figure 9 shows the specifications in red points, the experimental performance with the reference laser and the HiPPO laser, respectively in solid lines and dashed lines. From 10 Hz to 100 kHz, the optical link does not degrade the reference signal, whatever the distribution rank and whatever the laser source. For rank 64, the HiPPO laser brings a 3 dB improvement thanks to a higher output power, which allows for a margin (≈ 3 dB) compared with target specifications.

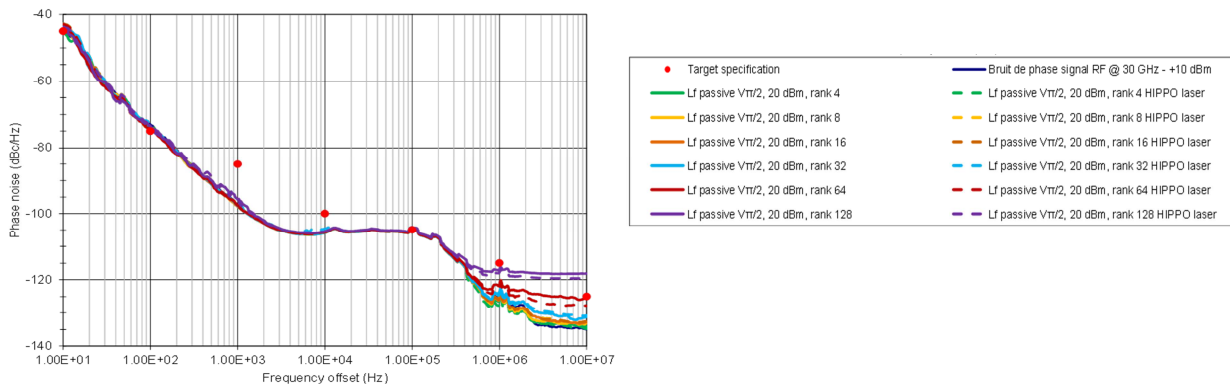


Figure 9. Optical LO distribution results: RF phase noise performance as a function of the distribution rank.

5.2 Photonic RF frequency conversion

One HiPPO laser module was evaluated in a photonic RF frequency conversion set-up with the objective to demonstrate Ka/Ka-band frequency-down conversion. Figure 10 shows the set-up partly reusing the demonstrator developed within the ESA OMCU (Optical Multi-frequency Conversion Unit) project.

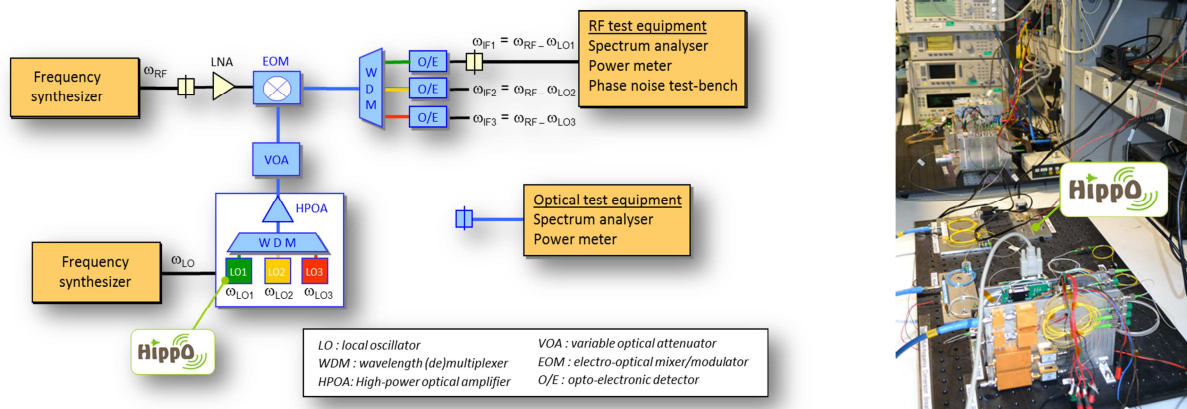


Figure 10. Photonic RF frequency-conversion set-up: (left) block diagram, (right) picture.

The number of LOs was reduced from 5 in the initial demonstrator to 3 for evaluation of the HiPPO laser. LO#1 was generated with one HiPPO laser with +20 dBm output power, whereas LO #2 and LO#4 were reused as they were. Optical LO's are generated from an RF LO with a MZM using dual-sideband modulation with carrier-suppression. The MZM being driven at a $F_{LO}/2$ frequency, and being biased for carrier extinction, an LO signal at F_{OL} is generating through the beating of the 2 side-bands. The LO #1 frequency was set at 9.3 GHz and the LO #2 and LO #4 frequencies both at 8.8 GHz. The RF power was about +18 dBm for all LOs. The RF signal to be down-converted was at 28.75 GHz so the IFs were respectively at 19.45 and 19.95 GHz. Similar performance in terms of optical spectrum and carrier suppression (close to -19 dB) were obtained with all LO independently of laser type.

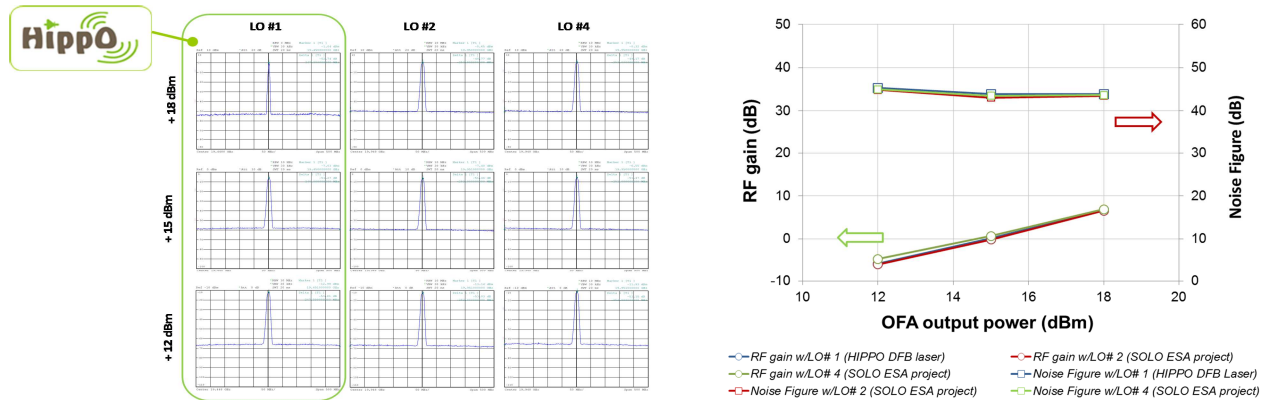


Figure 11. Photonic RF frequency-conversion performance: (left) output RF spectrum, (right) RF gain and noise figure.

The optical signal carrying the RF signals was amplified through an optical fibre amplifier (OFA), demultiplexed and detected. The frequency-conversion performance was assessed for 3 different OFA powers. Figure 11 (left) shows the RF spectrum at the RF output for each channel and each amplifier power. The output IF signal after frequency-conversion exhibited similar power and excellent purity in the 500 MHz bandwidth. The IF spectrum did not feature any unwanted mixing product higher than -50 dBc in the useful band. Figure 11 (right) gives the RF gain and noise figure performance for the 3 channels as a function of the OFA power. Same performance was obtained for the 3 channels. The RF gain is proportional to the OFA power whereas the NF is quasi-constant. The RF performances remains constant with the use of the HiPPO DFB laser module compared with state-of-the-art commercial high power DFB laser module.

5.3 Free-space optical communication test-bed

The applicability of HiPPO technology for free-space optical communication links was demonstrated using the fiber-based test-bed shown in Figure 12. Details about the test-bed can be found in ⁷.

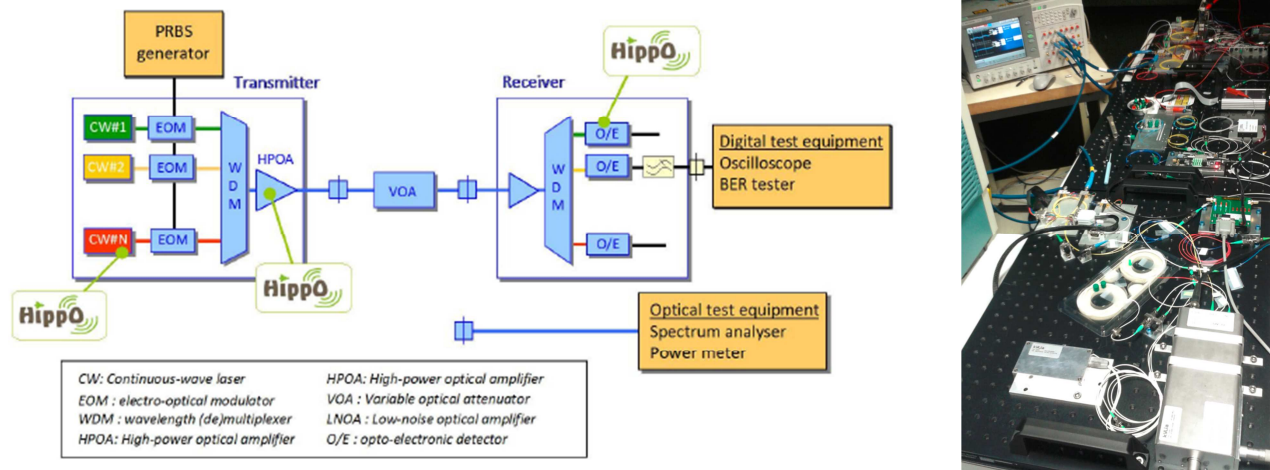


Figure 12. FSO communication set-up: (left) Block diagram, (right) Picture

Bit-error-rate (BER) measurements were first performed with a commercial laser from G & H, and then with an HiPPO laser with +17 dBm output power. The test-bed was configured for NRZ-OOK transmission at 10 Gb/s with $2^{31}-1$ PRBS data. Figure 13 shows the experimental curves. Quasi-error-free operation was obtained with no indication of any BER floor. No particular penalty was revealed when using the HiPPO laser compared to commercial parts.

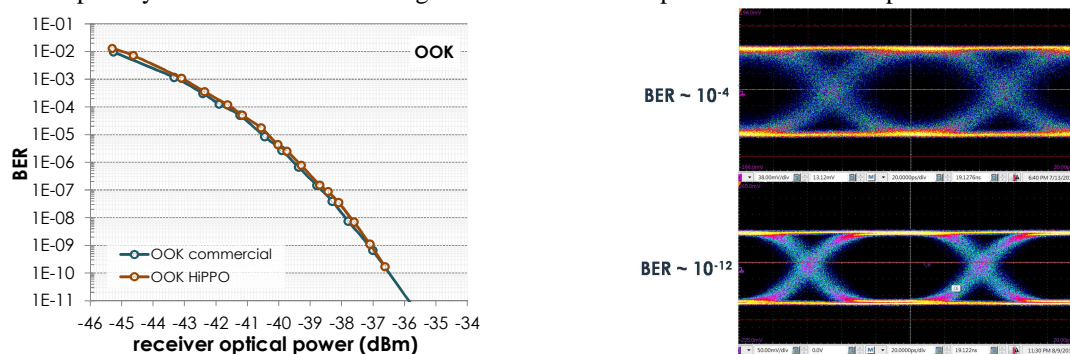


Figure 13. FSO communication results (a) BER curve, (b) Eye diagrams

6. CONCLUSION

A space-grade DFB laser module has been developed with up to 200 mW output power and very low noise. Laser chips and modules were tested in detail and submitted to environmental testing for proving their suitability for space. A sub-set of modules was implemented for system evaluation in laboratory test-beds representative of satellite-based applications. This included photonic distribution high-frequency (30 GHz) LO's, photonic RF frequency conversion with multiple LO's, and a free-space optical communication link at 10 Gb/s in OOK format. There was no particular degradation of system performance by using HiPPO laser modules compared with state-of-the-art commercial parts. This validates the functional performance of the space-grade HiPPO laser modules and their suitability for analog RF sub-systems and high-speed digital communications solutions in satellite-based applications.

ACKNOWLEDGEMENTS

This work was supported by the European Commission Directorate-General for Research and Innovation within the framework of the European Space Project HiPPO under Grant 606915. The authors also thank ESA and N. Karafolas as Technical Officer at ESTEC, for partial reuse of the OMCU (contract N. 21406/08/NL/EM) project demo, as well as CNES, the French national space agency, and its technical officer L. Gatet for reuse of the LO distribution test-bed (contract R&T CNES S15/TC-0007-079).

REFERENCES

- [1] Sotom, M. et al., "Flexible Photonic Payload for Broadband Telecom Satellites: from Concepts to System Demonstrators," Proc. ICSO 2016 (International Conference on Space Optics), Biarritz, France, 2016.
- [2] Faugeron, M. et al., "High-Power Tunable Dilute Mode DFB Laser With Low RIN and Narrow Linewidth," IEEE Photon. Technol. Lett., vol. 25, no. 1, pp. 7-10, Jan. 1, 2013.
- [3] Ishii, H., Kasaya, K., and Oohashi, H., "Wavelength-tunable Lasers for Next-generation Optical Networks," NTT Technical Review, vol. 9, no. 3, Mar. 2011.
- [4] Derickson, D., Fiber Optic Test and Measurement (Hewlett-Packard Professional Books). 1998, pp.179-202.
- [5] Mercer, L. B., "1/f Frequency Noise effects on self-Heterodyne Linewidth Measurements," IEEE J. Lightwave Technol., vol. 9, no. 4, pp. 485-493, Apr. 1991.
- [6] MacDougall, J. et al., "Optoelectronic Modules for Space Applications," Proc. ICSO 2016 (International Conference on Space Optics), Biarritz, France, 2016.
- [7] Maho, A. et al., "Assessment of the effective performance of DPSK vs. OOK in satellite-based optical communications," Proc. ICSO 2018 (International Conference on Space Optics), Chania, Greece, 2018.